Decoupling the conduction from redox reaction and electronic reconstruction at polar oxide interfaces

M. H. Li,[1,3,*] H. Li,[2,*] Y. L. Gan,[1] H. Xu,[1] C. M. Xiong,[3] F. X. Hu,[1] J. R. Sun,[1] T. Schmitt,[2] V. N. Strocov,[2,†] Y. Z. Chen,[1,‡] and B. G. Shen[1,4,5]

[1]*Beijing National Laboratory of Condensed Matter Physics and Institute of Physics, Chinese Academy of Sciences, Beijing 100190, China*
[2]*Swiss Light Source, Paul Scherrer Institute, 5232 Villigen-PSI, Switzerland*
[3]*Department of Physics, Beijing Normal University, Beijing 100875, China*
[4]*School of Physics, University of Chinese Academy of Sciences, Beijing 100049, China*
[5]*Ningbo Institute of Materials Technology & Engineering, Chinese Academy of Sciences, Ningbo, Zhejiang 315201, China*

(Received 5 December 2021; accepted 9 March 2022; published 30 March 2022)

The physical properties of oxide heterointerfaces depend crucially on the electronic and ionic reconstructions across the interface. For the formation of a two-dimensional electron liquid (2DEL) at the interface of $LaAlO_3/SrTiO_3$ (LAO/STO) systems, although it is well accepted that the conduction of amorphous-LAO/STO samples comes exclusively from the oxygen vacancies due to interfacial redox reactions, the relative contribution of ionic reconstruction and electronic reconstruction to the conduction at the polar crystalline LAO/STO interface has been a topic of debate. Herein, by resonant x-ray photoemission spectroscopy and x-ray absorption spectroscopy measurements, we investigated the evolution of the Ti $2p$ signal as well as the in-gap states at the diluted oxide interface of $LaAl_{1-x}Mn_xO_3$/STO ($0 \leqslant x \leqslant 0.3$), where the doping of Mn into LAO gradually decreases the carrier density of the interfacial 2DEL but does not change the interface polarity. The spectroscopic results present direct evidence that the conduction from redox reaction at polar LAO/STO interfaces is suppressed by increasing the Mn doping level without the need of oxygen postannealing. A pure polarity discontinuity induced electronic reconstruction can be achieved by deliberately controlling the Mn doping level in LAO, which results in low-carrier, high-mobility, and spin-polarized 2DELs at $x = 0.3$.

DOI: 10.1103/PhysRevMaterials.6.035004

I. INTRODUCTION

Heterostructures of transition metal oxides can exhibit a wide spectrum of astonishing properties and functionalities not accessible for their bulk counterparts, thanks to structural symmetry breaking and the strong coupling among spin, orbital, charge, and lattice degrees of freedom [1,2]. One of the particular emergent electronic phenomena is the formation of high-mobility two-dimensional electron liquids (2DELs) at the interface between two band insulators of $LaAlO_3$ and $SrTiO_3$ (LAO/STO) [3], which also exhibit magnetism [4,5], superconductivity [6,7], and quantum Hall effect [8]. Understanding the interface conduction mechanism has been one of the central issues of oxide electronics [9–15]; it consists of two fundamental aspects: (i) interfacial electronic reconstruction due to the polarity discontinuity; and (ii) interfacial ionic reconstructions—intermixing and/or chemical redox reactions. It has been generally accepted that the conduction mechanisms depend strongly on the growth oxygen pressure. For samples grown at low oxygen pressure (10^{-6} mbar) and high deposition temperature, conduction is dominated by oxygen vacancies (V_Os) which extend deeply into the substrate, while for samples grown at higher oxygen pressure (10^{-5}–10^{-3} mbar), the conduction is confined at the interface. However, considering the fact that redox reaction could occur at the interface between STO and the Al-containing oxides when oxygen pressure is below 10^{-3} mbar [16,17], for example, amorphous-LAO/STO (*a*-LAO/STO) [16], it remains open on the relative contribution of redox reaction, and thus V_Os and electronic reconstruction, to the interface conduction even though most of the carriers are confined at the interface (for samples grown at higher pressure of 10^{-5}–10^{-3} mbar) [13]. To resolve this issue, oxygen postannealing is often adopted but it results in either insulating or metallic interfaces [18], which is difficult to understand, firstly, due to the sensitivity of the STO conduction to the sample history and, secondly, because the electron mobility for the resultant 2DEL is often low.

Besides oxygen postannealing, interface engineering with the aim to decrease the content of V_Os on the STO side and to enhance the carrier mobility at LAO/STO interfaces has been intensively investigated [19–22]. One representative example is the incorporation of a surface strontium copper oxide nanolayer that enhances the oxygen surface exchanges and thus lowers the oxygen defects in STO as well as defect scattering at LAO/STO interfaces [19]. The other remarkable example is the introduction of a manganite buffer layer at the interface of *a*-LAO/STO [21] where the presence of $LaMnO_3$ (LMO) blocks the formation of V_Os in STO during the film deposition due to its high kinetic barrier for oxygen exchange [23], which results in a 2DEL with low carrier densities in the range of 10^{12} cm^{-2} and high mobility above

*These authors contributed equally to this work.
†vladimir.strocov@psi.ch
‡yzchen@iphy.ac.cn

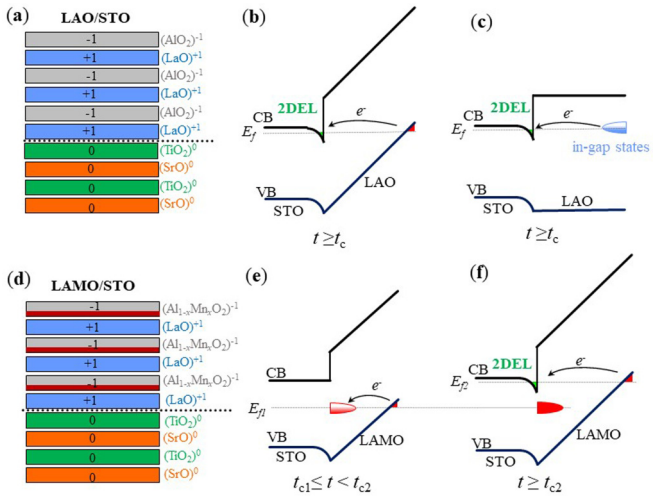

FIG. 1. Polar discontinuity and the intrinsic electronic reconstruction at the LAO/STO and LAMO/STO interfaces. (a), (d), Planar charge distribution across the polar interfaces. (b), (c) Schematic diagram for the formation of 2DELs at LAO/STO interface within the polar-catastrophe model and the surface defects model, respectively. (e), (f) Schematic diagram of the polar-catastrophe model at LAMO/STO interfaces.

$10\,000\,\mathrm{cm^2\,V^{-1}\,s^{-1}}$ at 2 K. In these engineered LAO/STO heterostructures, the charge transfer in addition to the formation of an interfacial 2DEL is determined by the interplay between polar discontinuities and redox reactions [10,12]. However, the relative contribution of redox reaction, and thus V_Os and electronic reconstruction, to the interface conduction remains to be investigated. Different from the cuprate-capped or manganite-buffered LAO/STO interfaces, the recent discovery of the diluted oxide interface, $LaAl_{1-x}Mn_xO_3$/STO (LAMO/STO) [22], enables us to tailor the carrier density and the ground state of the 2DEL deliberately in the full Mn doping range ($0 \leqslant x \leqslant 1$), where the carrier density is decreased gradually across the Lifshitz transition point of $n_c = 2.8 \times 10^{13}\,\mathrm{cm^{-2}}$ before it exhibits a sharp metal-insulator transition at $x = 0.3$. Compared to previous reports of diluting the LAO layer with nonpolar STO [24], the LAMO/STO system provides an opportunity to tune the carrier density of the interfacial 2DEL without changing the polar discontinuity across the interface, as demonstrated in Fig. 1. Herein, we further present spectroscopic evidence on the decoupling of the conduction from redox reaction and electronic reconstruction at LAMO/STO interfaces. Although the nonannealed LAO/STO interfaces exhibit conduction from both redox reaction and electronic reconstruction, the V_O-related in-gap states (IGS), and thus redox reaction at polar LAMO/STO interfaces, are suppressed by increasing the Mn dopant concentration in LAO. A pure polarity discontinuity induced electronic reconstruction is achieved by deliberately controlling the LMO doping level when the redox reaction on the STO side is strongly suppressed near $x = 0.3$, which results in low-carrier, high-mobility 2DELs.

II. EXPERIMENTAL METHODS

The LAMO/STO samples with Mn dopants of $x = 0$, 0.2, and 0.3 were grown on TiO_2-terminated STO substrates by pulse laser deposition (PLD) under 650 °C with O_2 pressure of approximately 3×10^{-5} mbar by ablating ceramic LAMO targets. The film thickness is fixed at 4 unit cells (u.c.) as determined by reflection high-energy electron diffraction (RHEED) intensity oscillations [22]. After the growth of the film, the sample was cooled under the same pressure at a rate of 15 °C/min to room temperature. Resonant x-ray photoemission spectroscopy (RXPS) measurements were performed at the ADRESS beamline [25] of the Swiss Light Source with photon energy of 1000 eV with C^+ polarization. The x-ray absorption spectroscopy (XAS) results across the Mn $L_{2/3}$ absorption edge were recorded in total-electron-yield mode. The photon energy varies from 630 to 660 eV at a step of 0.1 eV. The light had *s* polarization.

III. RESULTS AND DISCUSSION

Figure 1 illustrates the similarity and difference between the LAO/STO and LAMO/STO interfaces with respect to planar charge distribution and the electronic reconstructions. Referring to the intrinsic doping mechanism within the framework of the polar-catastrophe scenario, an electrostatic potential builds up as a function of LAO or LAMO thickness and pure electronic reconstruction induced 2DEL occurs as the film thickness is above a critical thickness t_c, where the valence O $2p$ band of LAO or LAMO at the surface is lifted up to the level of the STO Ti $3d$ conduction band at the interface [Figs. 1(b) and 1(f)] [26]. Experimentally, t_c is found to be 4 u.c. for the LAO/STO [27]. At and above t_c, electrons will migrate progressively from the surface to the interface, forming the 2DEL. The main difference between LAMO/STO and LAO/STO is the presence of the IGS which is related to the Mn e_g^2 subband lying below the conduction band of STO [28,29]. Therefore, there will be two critical thickness t_{c1} and t_{c2}, corresponding to the charge transfer to the empty Mn dopant e_g^2 subband correlated IGS and the STO Ti t_{2g} conduction band, respectively. At $t_{c1} \leqslant t < t_{c2}$, the electronically reconstructed electrons will be donated and trapped on the Mn sites [Fig. 1(e)], canceling part of the built-in polar field (depending on the Mn doping level) while contributing negligibly to the conduction. The critical thickness is determined by $t_c = (\varepsilon_0 \varepsilon_{\mathrm{LAMO}} \Delta E)/(e P^0_{\mathrm{LAMO}})$ [24]. Here, ε_0 is the permittivity of the vacuum, $\varepsilon_{\mathrm{LAMO}}$ is the relative permittivity of LAMO, e is the elementary charge, P^0_{LAMO} is the formal polarization of LAMO, and ΔE is the difference of energy between the valence band of LAMO and the conduction band of STO. For a typical LAO/STO case ($x = 0$), the $\Delta E \approx 3.3$ eV, and yields an estimate of $t_c^{\mathrm{LAO}} \approx 3.5$ u.c., in good agreement with the experimental value of $t_c = 4$ u.c. [27]. For the conducting LAMO/STO case ($0 < x \leqq 0.3$), where the Mn doping is low, the relative permittivity of the LAMO film can be approximately equal to $\varepsilon_{\mathrm{LAO}}$, and the key difference is that the electron trap states of Mn $3d$ e_g^2 levels lie approximately 0.7 eV below the conduction band of STO [28,29]. Therefore, $t_{c1} \approx 2.8$ u.c. Once the e_g^2 levels are filled (Mn^{3+} turns to Mn^{2+}), the electrostatic potential continues to diverge as the LAMO film increases, and subsequent electrons will be transferred to the conduction band of STO at a critical thickness t_{c2}, slightly larger than that of LAO/STO [Fig. 1(f)], i.e., $t_{c2} > 3.5$ u.c. Experimentally, t_{c2}

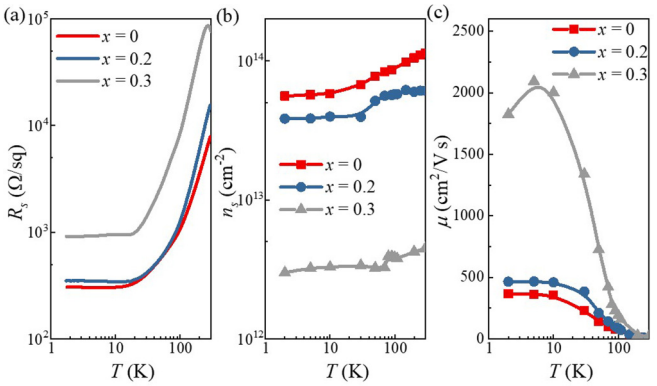

FIG. 2. (a)–(c) The temperature dependence of the sheet resistance (R_s), carrier density (n_s), and carrier mobility (μ) of the studied samples with Mn doping concentrations of $x = 0$, 0.2, and 0.3, respectively.

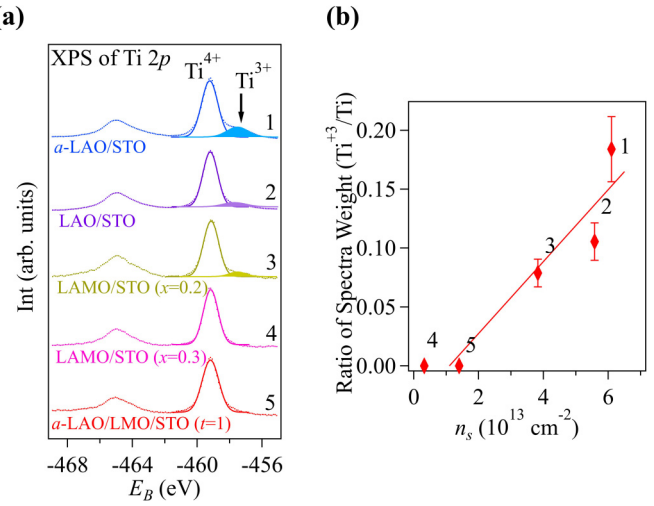

FIG. 3. (a) Ti 2p orbital XPS curves of LAO/STO, LAMO/STO ($x = 0.2$, 0.3), a-LAO/STO, and a-LAO/LMO/STO ($t = 1$, 2 u.c.). (b) Ratio of spectra weight between Ti^{3+} and Ti as a function of carrier density.

is also found to be 4 u.c. for LAMO/STO heterointerfaces at $0 \leqslant x \leqslant 0.3$ [22]. When x>0.3, the interface of LAMO/STO becomes highly insulating, probably due to the fact that most of the reconstructed electrons are accumulated on the Mn dopants. Note that there has been no detectable built-in potential of the order of the STO band gap at the LAO/STO interface [30]; therefore a modified scenario that polarity induced V_Os at the LAO surface serves as a charge reservoir for the electronic reconstruction is proposed [Fig. 1(c)] [30]. On the other hand, compared to the intensively investigated LAO/STO interfaces, the charge reconstruction and practical conduction mechanism at the LAMO/STO interface remains under investigation.

Figures 2(a)–2(c) show the temperature dependence of the sheet resistance (R_s), carrier density (n_s), and carrier mobility (μ) at different Mn doping concentrations of $x = 0$, 0.2, and 0.3, respectively. All three samples are metallic. The metallic LAO/STO is characterized by a typical sheet carrier density $n_s = 1.1 \times 10^{14}\,\mathrm{cm}^{-2}$ measured by Hall effect at room temperature ($T = 300\,\mathrm{K}$). At a low temperature of 2 K, n_s of $5.58 \times 10^{13}\,\mathrm{cm}^{-2}$ and a typical electron mobility μ of $367\,\mathrm{cm}^2\,\mathrm{V}^{-1}\,\mathrm{s}^{-1}$ are obtained. Increasing the Mn doping level reduces the carrier density and causes the gradual increase of sheet resistance, which is in good agreement with the electron sink effect described in Figs. 1(e) and 1(f). At $x = 0.2$, the carrier density is $3.83 \times 10^{13}\,\mathrm{cm}^{-2}$ at 2 K which remains higher than the Lifshitz transition point of $n_c = 2.8 \times 10^{13}\,\mathrm{cm}^{-2}$ [22]. This means the conduction of both LAO/STO and LAMO/STO ($x = 0.2$) lies in the two-band conduction region where both Ti t_{2g} d_{xy} electrons and d_{xz}/d_{yz} electrons contribute to the conduction. In contrast, the LAMO/STO ($x = 0.3$) samples exhibit a carrier density of $3.2 \times 10^{12}\,\mathrm{cm}^{-2}$, which is much lower than n_c and also lower than the carrier density for the single-unit-cell LMO buffered a-LAO/STO interface [21]. Therefore, the conduction of LAMO/STO ($x = 0.3$) lies in the single-band conduction region with mainly d_{xy} electrons contributing to the conduction, while their low-temperature mobility is enhanced by 3–4 times compared to the LAO/STO, probably due to the Lifshitz transition. It is noteworthy that a clear anomalous Hall effect is also observed at $x = 0.3$, which indicates the 2DEL is spin polarized. Additionally, the temperature dependence of the resistivity of the LAMO/STO at $x = 0.3$ shows a clear discontinuity around $T = 20\,\mathrm{K}$. Considering the fact that there is no discontinuity in the temperature dependent carrier density (n_s) at $T = 20\,\mathrm{K}$ [Fig. 2(b)], the resistivity discontinuity is mainly due to the change in the carrier mobility (μ), where we did observe a clear decrease in the mobility around 10 K [Fig. 2(c)]. The low-temperature mobility of $SrTiO_3$ is mainly determined by defect scattering. When the LMO doping level is relatively high (such as $x = 0.3$, the highest doping level for a conducting sample), there is more La interdiffusion and/or Ti/Mn intermixing into $SrTiO_3$ expected [22], so the resistivity shows a slight upturn at $T = 20\,\mathrm{K}$. Note that the onset of the measured magnetic signal, particularly the anomalous Hall effect, becomes only clear at $T = 2\,\mathrm{K}$, so the relation is weak between the discontinuity in the resistivity and the magnetic signal. The typical low-temperature transport properties of LAMO/STO ($x = 0$, 0.2, and 0.3) samples are also summarized in Table I. For comparison, the results of the a-LAO/STO system where the conduction is dominated by the redox reaction induced V_Os are also presented.

The transport measurements detect mainly the mobile 2DEL electrons. In contrast, optical and spectroscopic measurements detect simultaneously both mobile and localized 3d electrons at the interface, and thus the total reconstructed electrons [30–33]. In particular, RXPS can enhance the spectral weight of Ti 3d states around the Fermi level position and thus has been widely used to study the interface electronic structure of LAO/STO heterostructures [32,33]. By scanning the photon energies across the Ti 2p core level, RXPS can distinguish if the interface carriers are associated with the in-gap states resulting from V_Os or the quasiparticle states from 2DELs. Figure 3 shows the Ti 2p spectra of the series samples of LAMO/STO ($x = 0$, 0.2, 0.3) in addition to the a-LAO/STO interfaces. The amorphous a-LAO/STO, where the conduction is dominated exclusively by redox reactions, shows a clear signature of Ti^{3+} near the binding energy of 458 eV, indicating the presence of a

TABLE I. Summary of low-temperature carrier density (n_s), carrier mobility (μ), and the relative concentration of the Ti^{3+} of the studied samples.

Samples	LAO/STO	LAMO/STO $x = 0.2$	LAMO/STO $x = 0.3$	*a*-LAO/STO	*a*-LAO/LMO/STO
n_s (10^{13} cm^{-2})	5.58	3.83	0.32	6.0	1.4
μ (cm^2 V^{-1} s^{-1})	367	464	1698	220	4392
Ti^{3+} percentage	~0.11	~0.08	~0	~0.19	~0

large amount of V_Os on the STO side. The estimated percentage of Ti^{3+} is 0.19%, corresponding to a carrier density of 1.33×10^{14} cm^{-2}, higher than that measured by the Hall effect, as expected, because the electrons released by the V_Os tend to form clusters of localized states, in particular, at high V_O concentrations [32]. Although the *a*-LAO/STO and the crystalline LAO/STO show comparable carrier density from transport measurement, the crystalline LAO/STO only shows a finite signature of Ti^{3+} and its percentage is decreased approximately two times to 0.11% compared to the *a*-LAO/STO. This indicates that the interfacial redox reaction contributes less to the 2DEL at crystalline LAO/STO despite the absence of oxygen postannealing, probably due to oxygen uptake from the background during the high-temperature deposition. It further highlights that the conduction mechanisms are different between LAO/STO and *a*-LAO/STO [13]. Upon Mn doping, a significant decrease in Ti^{3+} at the LAMO/STO interfaces is observed and, at $x = 0.3$, the content of Ti^{3+} becomes so low that it is beyond the detection limit of our RXPS measurement. Therefore, the contribution of the V_Os to the interface conduction is expected to be negligible at $x = 0.3$. Figure 2 summarizes the ratio of spectra weight of Ti^{3+} ($I(Ti^{3+})/[I(Ti^{3+}) + I(Ti^{4+})]$) with respect to the sheet carrier density, n_s, measured by Hall effect at 2 K. It is remarkable that the content of the Ti^{3+} scales with the n_s for *a*-LAO/STO, and crystalline LAO/STO and LAMO/STO ($x = 0.2$) when $n_s \geqslant 1.1 \times 10^{13}$ cm^{-2}. This probably suggests a high limit for the pure polar discontinuity induced 2DELs at the LAO/STO interfaces; i.e., the LAO/STO interface with $n_s \leqslant 1.1 \times 10^{13}$ cm^{-2} will come predominantly from intrinsic electronic reconstruction as observed in *a*-LAO/LMO/STO ($t = 1$ u.c.) [12,21]. This limit is also in good agreement with that achieved in the $SrCuO_2$-capped defect-free LAO/STO [19]. When $n_s > 1.1 \times 10^{13}$ cm^{-2}, the interface conduction most likely comes from both polarity discontinuity induced electronic reconstruction and the interfacial redox reactions.

Figure 4(a) shows the Mn *L* edge XAS for the LAMO/STO as well as the *a*-LAO/STO buffered with 1 u.c. LMO. Strong features near 640 eV appear in the XAS spectra at the Mn *L* edge for both diluted interfaces of LAMO/STO with $x = 0.2$ and $x = 0.3$, which corresponds to the main absorption peak of Mn^{2+} as observed in buffered *a*-LAO/LMO/STO ($t = 1$ u.c.) [21,34,35]. Therefore, the nominal valence of the Mn^{3+} dopant is strongly or completely reduced to Mn^{2+} in diluted heterostructures of LAMO/STO ($x = 0.2, 0.3$) [12,21]. This is consistent with the scenario that during the formation of a 2DEL in the buffered and diluted samples, the electrons will be first transferred to the Mn sublattice before filling the electronic shell of Ti ions, as illustrated in Figs. 1(e) and 1(f). The observed decrease in both Ti^{3+} concentration and the Hall carrier density as presented in Fig. 3 should result from such electron sink effect of the Mn dopant and/or the suppression of formation of V_Os in STO.

To further investigate the effect of the Mn dopant on the interfacial redox reaction or formation of V_Os in STO, we identified the V_O-related IGS through the photoemission spectra. If there are V_Os on the STO side, strong electron redistribution on neighboring Ti^{4+} is expected. Besides the contribution to the 2DEL, a large fraction of electrons released by the V_Os (half, in the ideal case) stays near the Ti ion to form there a localized IGS (Ti-IGS) at binding energy $E_B \sim -1.3$ eV, which is Ti e_g derived (see Appendix), strongly correlated, magnetic, and is often viewed as a small polaron [32,33,36]. This characteristic signature could therefore provide direct evidence of V_Os on the STO side of the LAO/STO and LAMO/STO interfaces. Figure 4(b) shows the evolution of the Ti-IGS as a function of Mn doping in LAMO/STO ($x = 0$, 0.2, 0.3) measured at $h\nu = 464.4$ eV, which boosts the Ti-IGS peak. This peak is relatively large for our LAO/STO and thus the nonannealed LAO/STO is slightly oxygen deficient. It also confirms the main contribution of V_O to the interface conduction. As the Mn dopant concentration is increased to $x = 0.2$, the V_O-related Ti-IGS peak strongly decreases, manifesting the suppressed redox reaction upon the Mn doping. At the same time, a new IGS peak related

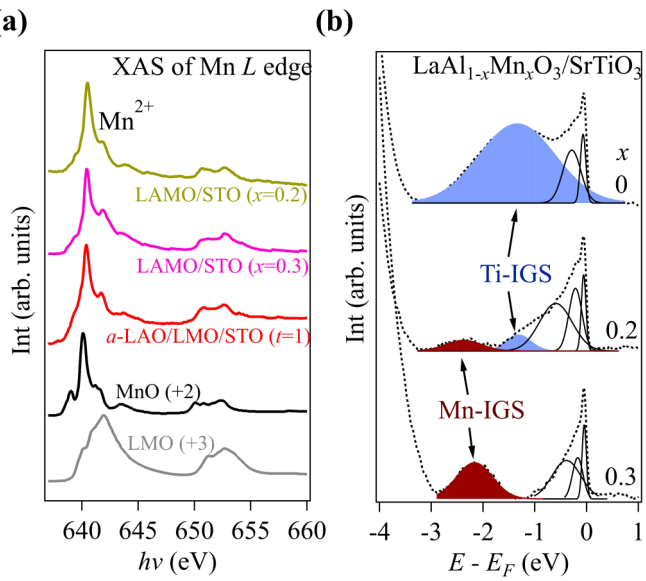

FIG. 4. (a) XAS spectra at the Mn *L* edge of LAMO/STO ($x = 0.2$, 0.3), spectra of *a*-LAO/LMO/STO ($t = 1$ u.c.) [21]; reference materials MnO (Mn^{2+}) and LaMnO3 (Mn^{3+}) are also shown for comparison. (b) Spectra measured through the whole valence band at $h\nu = 464.4$ eV boosting the V_O-related IGS peaks.

to the Mn dopant (Mn-IGS) is also observed at $E_B \sim -2$ eV (see Appendix). As the Mn dopant concentration increases to $x = 0.3$, the V_O-related Ti-IGS peak reduces while the Mn-IGS peak builds up. The above results strongly suggest that the Mn dopant plays two critical roles: firstly, it acts as an electron sink; secondly, it prevents the formation of V_Os on the STO side. These unique features make it possible to decouple the conduction from redox reaction and intrinsic electronic reconstructions.

IV. CONCLUSION

In summary, we have investigated the charge reconstruction at the diluted oxide interface of $LaAl_{1-x}Mn_xO_3$/STO ($0 \leqslant x \leqslant 0.3$) by resonant x-ray photoemission spectroscopy and x-ray absorption spectroscopy measurements. A linear relationship is observed between the reconstructed electrons with respect to 2DEL carrier density, which indicates a high limit for the pure polar discontinuity induced 2DELs at LAO/STO interfaces, $n_s = 1.1 \times 10^{13}$ cm^{-2}. A decrease of oxygen-vacancy-related in-gap states upon increasing the Mn doping level is also observed, manifesting that the conduction from redox reaction at polar LAO/STO interfaces is suppressed by increasing the Mn doping level without the need of oxygen postannealing. The results strongly suggest that pure polarity discontinuity induced electronic reconstruction can be achieved by deliberately controlling the Mn doping level in LAO to remove the contribution from the V_Os.

ACKNOWLEDGMENTS

The authors acknowledge the support from the National Key Research and Development Program of China (Grant No. 2021YFA1400300), the Science Center of the National Science Foundation of China (Grant No. 52088101), and the Strategic Priority Research Program (B) of the Chinese Academy of Sciences (Grant No. XDB33030200). J.R.S. expresses thanks for the support of the Project for Innovative Research Team of the National Natural Science Foundation of China (Grant No. 111921004).

APPENDIX

See Fig. 5, which shows RXPS data across the Mn and Ti L edges, identifying the Mn-derived and Ti-derived in-gap states (Mn-IGS and Ti-IGS, respectively).

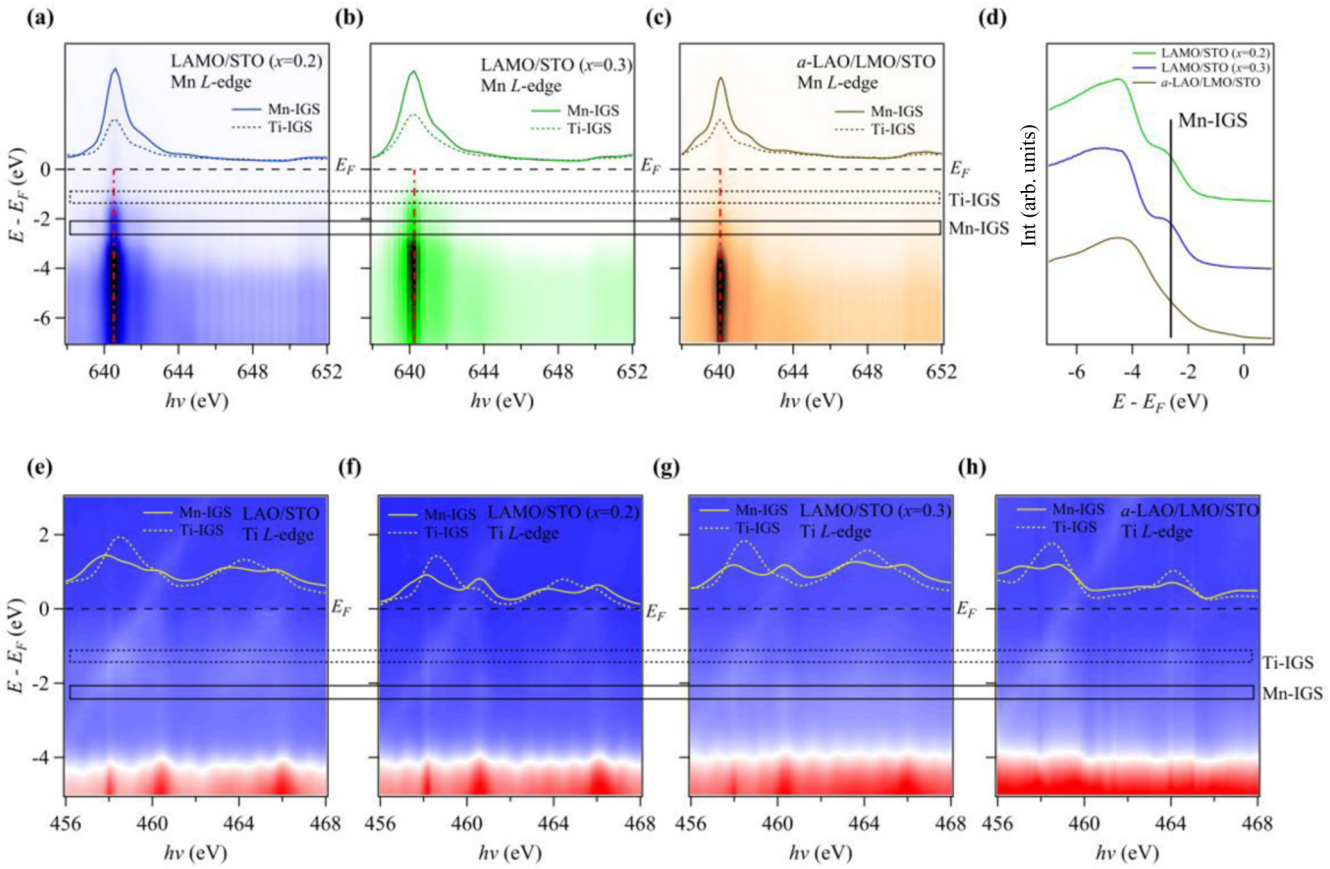

FIG. 5. (a)–(c) Angle-integrated RXPS intensity map at the Mn L edge for LAMO/STO ($x = 0.2$, 0.3) and a-LAO/LMO/STO, respectively. The solid curve shows the intensity of the Mn-IGS at -2 eV, whose strong resonance identifies its predominantly Mn character. The dashed curve displays the Ti-IGS at -1.3 eV, whose weaker but significant intensity enhancement reveals an admixture of the Mn character. (d) Energy distribution curves (EDCs) extracted from (a–c) at the main Mn resonance peak at ~640 eV. (e–h) Angle-integrated RXPS intensity map at the Ti L edge for LAO/STO, LAMO/STO ($x = 0.2/0.3$), and a-LAO/LMO/STO, respectively. The yellow solid and dashed curves show intensities of the Mn-IGS and Ti-IGS, respectively. Whereas the strong resonance of the Ti-IGS confirms its predominantly Ti character, the resonance of the Mn-IGS identifies an admixture of the Ti character in it. The horizontal solid and dashed lines through the maps mark the energy integration windows for the Mn-IGS and Mn-IGS, respectively.

[1] H. Y. Hwang, Y. Iwasa, M. Kawasaki, B. Keimer, N. Nagaosa, and Y. Tokura, Nat. Mater. **11**, 103 (2012).

[2] Z. Huang, Ariando, X. R. Wang, A. Rusydi, J. S. Chen, H. Yang, and T. Venkatesan, Adv. Mater. **30**, 1802439 (2018).

[3] A. Ohtomo and H. Y. Hwang, Nature (London) **427**, 423 (2004).

[4] A. Brinkman, M. Huijben, M. van Zalk, J. Huijben, U. Zeitler, J. C. Maan, W. G. van der Wiel, G. Rijnders, D. H. Blank, and H. Hilgenkamp, Nat. Mater. **6**, 493 (2007).

[5] D.-S. Park, A. D. Rata, I. V. Maznichenko, S. Ostanin, Y. L. Gan, S. Agrestini, G. J. Rees, M. Walker, J. Li, J. Herrero-Martin, G. Singh, Z. Luo, A. Bhatnagar, Y. Z. Chen, V. Tileli, P. Muralt, A. Kalaboukhov, I. Mertig, K. Dörr, A. Ernst, and N. Pryds, Nat. Commun. **11**, 3650 (2020).

[6] N. Reyren, S. Thiel, A. D. Caviglia, L. Fitting Kourkoutis, G. Hammerl, C. Richter, C. W. Schneider, T. Kopp, A.-S. Rüetschi, D. Jaccard, M. Gabay, D. A. Muller, J. M. Triscone, and J. Mannhart, Science **317**, 1196 (2007).

[7] G. Herranz, G. Singh, N. Bergeal, A. Jouan, J. Lesueur, J. Gazquez, M. Varela, M. Scigaj, N. Dix, F. Sanchez, and J. Fontcuberta, Nat. Commun. **6**, 6028 (2015).

[8] F. Trier, G. E. D. K. Prawiroatmodjo, Z. Zhong, D. V. Christensen, M. von Soosten, A. Bhowmik, J. M. García Lastra, Y. Chen, T. S. Jespersen, and N. Pryds, Phys. Rev. Lett. **117**, 096804 (2016).

[9] M.-A. Rose, B. Šmíd, M. Vorokhta, I. Slipukhina, M. Andrä, H. Bluhm, T. Duchoň, M. Ležaić, S. A. Chambers, R. Dittmann, D. N. Mueller, and F. Gunkel, Adv. Mater. **33**, 2004132 (2021).

[10] R. J. Green, V. Zabolotnyy, M. Zwiebler, Z. Liao, S. Macke, R. Sutarto, F. He, M. Huijben, G. Rijnders, G. Koster, J. Geck, V. Hinkov, and G. A. Sawatzky, Phys. Rev. Mater. **5**, 065004 (2021).

[11] S. A. Chambers, L. Qiao, T. C. Droubay, T. C. Kaspar, B. W. Arey, and P. V. Sushko, Phys. Rev. Lett. **107**, 206802 (2011).

[12] Y. Z. Chen, R. J. Green, R. Sutarto, F. He, S. Linderoth, G. A. Sawatzky, and N. Pryds, Nano Lett. **17**, 7062 (2017).

[13] Z. Q. Liu, C. J. Li, W. M. Lu, X. H. Huang, Z. Huang, S. W. Zeng, X. P. Qiu, L. S. Huang, A. Annadi, J. S. Chen, J. M. D. Coey, T. Venkatesan, and Ariando, Phys. Rev. X **3**, 021010 (2013).

[14] F. Gunkel, D. V. Christensen, Y. Z. Chen, and N. Pryds, Appl. Phys. Lett. **116**, 120505 (2020).

[15] Y. Z. Chen, F. Trier, T. Kasama, D. V. Christensen, N. Bovet, Z. I. Balogh, H. Li, K. Thyden, W. Zhang, S. Yazdi, P. Norby, N. Pryds, and S. Linderoth, Nano Lett. **15**, 1849 (2015).

[16] Y. Chen, N. Pryds, J. E. Kleibeuker, G. Koster, J. R. Sun, E. Stamate, B. G. Shen, G. Rijnders, and S. Linderoth, Nano Lett. **11**, 3774 (2011).

[17] K. J. Kormondy, A. B. Posadas, T. Q. Ngo, S. Lu, N. Goble, J. Jordan-Swee, X. P. A. Gao, D. J. Smith, M. R. McCartney, J. G. Ekerdt, and A. A. Demkov, J. Appl. Phys. **117**, 095303 (2015).

[18] A. Kalabukhov, R. Gunnarsson, J. Börjesson, E. Olsson, T. Claeson, and D. Winkler, Phys. Rev. B **75**, 121404(R) (2007).

[19] M. Huijben, G. Koster, M. K. Kruize, S. Wenderich, J. Verbeeck, S. Bals, E. Slooten, B. Shi, H. J. A. Molegraaf, J. E. Kleibeuker, S. van Aert, J. B. Goedkoop, A. Brinkman, D. H. A. Blank, M. S. Golden, G. van Tendeloo, H. Hilgenkamp, and G. Rijnders, Adv. Funct. Mater. **23**, 5240 (2013).

[20] Y. Xie, C. Bell, Y. Hikita, S. Harashima, and H. Y. Hwang, Adv. Mater. **25**, 4735 (2013).

[21] Y. Z. Chen, F. Trier, T. Wijnands, R. J. Green, N. Gauquelin, R. Egoavil, D. V. Christensen, G. Koster, M. Huijben, N. Bovet, S. Macke, F. He, R. Sutarto, N. H. Andersen, J. A. Sulpizio, M. Honig, G. E. D. K. Prawiroatmodjo, T. S. Jespersen, S. Linderoth, S. Ilani *et al.*, Nat. Mater. **14**, 801 (2015).

[22] Y. L. Gan, D. V. Christensen, Y. Zhang, H. R. Zhang, D. Krishnan, Z. Zhong, W. Niu, D. J. Carrad, K. Norrman, M. von Soosten, T. S. Jespersen, B. G. Shen, N. Gauquelin, J. Verbeeck, J. R. Sun, N. Pryds, and Y. Z. Chen, Adv. Mater. **31**, 1805970 (2019).

[23] Y. Z. Chen, M. Döbeli, E. Pomjakushina, Y. L. Gan, N. Pryds, and T. Lippert, Phys. Rev. Mater, **1**, 052002(R) (2017).

[24] M. L. Reinle-Schmitt, C. Cancellieri, D. Li, D. Fontaine, M. Medarde, E. Pomjakushina, C. W. Schneider, S. Gariglio, Ph. Ghosez, J.-M. Triscone, and P. R. Willmott, Nat. Commun. **3**, 932 (2012).

[25] V. N. Strocov, X. Wang, M. Shi, M. Kobayashi, J. Krempasky, C. Hess, T. Schmitt, and L. Patthey, J. Synchrotron Radiat. **21**, 32 (2014).

[26] Y. Z. Chen and N. Pryds, Nat. Mater. **17**, 215 (2018).

[27] S. Thiel, G. Hammerl, A. Schmehl, C. W. Schneider, and J. Mannhart, Science **313**, 1942 (2006).

[28] A. Sawa, A. Yamamoto, H. Yamada, T. Fujii, M. Kawasaki, J. Matsuno, and Y. Tokura, Appl. Phys. Lett. **90**, 252102 (2007).

[29] Y. Z. Chen, J. R. Sun, A. D. Wei, W. M. Lu, S. Liang, and B. G. Shen, Appl. Phys. Lett. **93**, 152515 (2008).

[30] G. Berner, M. Sing, H. Fujiwara, A. Yasui, Y. Saitoh, A. Yamasaki, Y. Nishitani, A. Sekiyama, N. Pavlenko, T. Kopp, C. Richter, J. Mannhart, S. Suga, and R. Claessen, Phys. Rev. Lett. **110**, 247601 (2013).

[31] M. Sing, G. Berner, K. Goß, A. Muller, A. Ruff, A. Wetscherek, S. Thiel, J. Mannhart, S. A. Pauli, C. W. Schneider, P. R. Willmott, M. Gorgoi, F. Schafers, and R. Claessen, Phys. Rev. Lett. **102**, 176805 (2009).

[32] V. N. Strocov, A. Chikina, M. Caputo, M.-A. Husanu, F. Bisti, D. Bracher, T. Schmitt, F. Miletto Granozio, C. A. F. Vaz, and F. Lechermann, Phys. Rev. Mater. **3**, 106001 (2019).

[33] A. Chikina, D. V. Christensen, V. Borisov, M.-A. Husanu, Y. Chen, X. Wang, T. Schmitt, M. Radovic, N. Nagaosa, A. S. Mishchenko, R. Valentí, N. Pryds, and V. N. Strocov, ACS Nano **15**, 4347 (2021).

[34] M. Abbate, F. M. F. de Groot, J. C. Fuggle, A. Fujimori, O. Strebel, F. Lopez, M. Domke, G. Kaindl, G. A. Sawatzky, M. Takano, Y. Takeda, H. Eisaki, and S. Uchida, Phys. Rev. B **46**, 4511 (1992).

[35] Z. Chen, Z. Chen, Z. Q. Liu, M. E. Holtz, C. J. Li, X. Renshaw Wang, W. M. Lü, M. Motapothula, L. S. Fan, J. A. Turcaud, L. R. Dedon, C. Frederick, R. J. Xu, R. Gao, A. T. N'Diaye, E. Arenholz, J. A. Mundy, T. Venkatesan, D. A. Muller, L.-W. Wang *et al.*, Phys. Rev. Lett. **119**, 156801 (2017).

[36] A. Chikina, F. Lechermann, M.-A. Husanu, M. Caputo, C. Cancellieri, X. Wang, T. Schmitt, M. Radovic, and V. N. Strocov, ACS Nano **12**, 7927 (2018).